



Cite this: *Nanoscale*, 2020, **12**, 9717

Enhanced motility in a binary mixture of active nano/microswimmers†

Debajyoti Debnath,^a Pulak Kumar Ghosh,^a Vyacheslav R. Misko,^{b,c} Yunyu Li,^d Fabio Marchesoni^{d,e} and Franco Nori^{b,f}

It is often desirable to enhance the motility of active nano- or microscale swimmers such as, e.g., self-propelled Janus particles as agents of chemical reactions or weak sperm cells for better chances of successful fertilization. Here we tackle this problem based on the idea that motility can be transferred from a more active guest species to a less active host species. We performed numerical simulations of motility transfer in two typical cases, namely for interacting particles with a weak inertia effect, by analyzing their velocity distributions, and for interacting overdamped particles, by studying their effusion rate. In both cases, we detected motility transfer with a motility enhancement of the host species of up to a factor of four. This technique of motility enhancement can find applications in chemistry, biology and medicine.

Received 2nd March 2020,
Accepted 15th March 2020

DOI: 10.1039/d0nr01765e

rsc.li/nanoscale

1. Introduction

Self-propelling Janus particles (JPs), the most common class of artificial microswimmers, have been the focus of widespread attention over the last two decades due to their emerging applications in nano-technology and medical science.^{1–7} Such particles are made by coating one hemisphere with catalytic or photo-sensitive or magnetic materials.^{1,2,4} Under appropriate conditions, one hemisphere undergoes physical or chemical changes with respect to the other, thus producing some local gradient in the suspension fluid (self-phoresis). This strategy allows artificial swimmers to propel themselves by harvesting energy from their environment.

Thanks to their self-propulsion mechanism and in contrast to their passive peer, artificial swimmers can diffuse orders of magnitude faster,⁸ are capable of performing autonomous motion in periodic structures with broken spatial symmetry^{9–12} and exhibit other peculiar transport properties.^{13–17} Inspired by these unique transport features, researchers aim to design

customized JPs to be used, for instance, as “nano-robots” capable of performing accurate mechanical operations.^{18–23} Additional promising technological applications have also been proposed.^{1,9,24,32,33} Among the most appealing ideas being pursued, we mention here the recent attempt to power passive particles through the self-propulsion mechanism of intermediary active particles,^{9,31–35} to be used as controllable stirrers. In this paper, we numerically study the velocity distribution and effusion of active particles in a binary mixture, to understand how to enhance motility of less active particles by adding more active particles. Mixtures of interacting active particles (either of the same or different kinds) behave quite differently in many ways. For dilute solutions, particles interact *via* long-range hydrodynamic flows generated by active particles and the short-range interactions can be safely ignored.⁶ However, transport properties of dense mixtures are mostly dominated by the short-range interactions, which are responsible for a variety of cluster and pattern formation processes reported in the recent literature.^{25–28}

Our simulation of binary active mixtures shows that adding a fraction of active microswimmers, such as self-propelled JPs, to a suspension of passive colloidal particles, results in a motility increase of the latter species. However, adding a small fraction of more active particles to a suspension of less active microswimmers results in a non-trivial behavior, whereby the added species appears to enhance the motility of the host species. Such a mechanism can be controlled by tuning the parameters of the guest species, e.g., the intensity of light in the case of light-induced JPs using laser beams,³⁶ near-infrared light³⁷ or visible light.^{38,39}

Our findings can be potentially useful for various chemical, biological and medical applications. For example, this tech-

^aDepartment of Chemistry, Presidency University, 86/1 College Street, Kolkata 700073, India. E-mail: pulak.chem@presiuniv.ac.in

^bTheoretical Quantum Physics Laboratory, RIKEN Cluster for Pioneering Research, Wako-shi, Saitama 351-0198, Japan

^c μ Flow group, Department of Chemical Engineering, Vrije Universiteit Brussel, Pleinlaan 2, 1050 Brussels, Belgium. E-mail: veaceslav.misco@vub.be

^dCenter for Phononics and Thermal Energy Science, School of Physics Science and Engineering, Tongji University, Shanghai 200092, People's Republic of China

^eIstituto Nazionale di Fisica Nucleare, Sezione di Perugia, I-06123 Perugia, Italy

^fDepartment of Physics, University of Michigan, Ann Arbor, Michigan 48109-1040, USA

†Electronic supplementary information (ESI) available. See DOI: 10.1039/D0NR01765E

nique could be used to increase the rate of *in vitro* fertilization by enhancing the motility of weak sperm cells. The same strategy can be implemented in a chemical reactor to govern the reaction rate, whereby one adds inert active particles to stir otherwise slowly diffusing reactant molecules.

Furthermore, it should be noted that the motility transfer mechanism is associated with some correlated particle dynamics in the mixture. The most sophisticated way to quantify motion correlation of weak and strong active particles is to compute the mixture cooperativity.⁴⁹ However, we focus here on the role of cooperativity in controlling the velocity distribution and effusion rates of weak JPs *via* motility transfer.

The outline of the paper is as follows. In section 2, we present a simple dynamical model for interacting self-propelling JPs in two dimensions, which we implemented in our numerical simulation code. In section 3, we explore the velocity distributions of the two mixture components. We consider first the case of a mixture of two identical species (single species case), of noninteracting, section 3.1, or interacting particles, section 3.2, and, then, the general case of a binary mixture of two different species of interacting active JPs. In section 4, we report our data for the effusion rates of the two JP species out of a narrow opening of the simulation box. Finally, in section 5 we draw a few concluding remarks.

2. Model

Let us consider a two-dimensional system consisting of two types of JPs with different self-propulsion speeds in a thermal bath: N_w with speed v_w and N_s with speed v_s . In the following, we will refer the subscripts 's' and 'w' to "strong" and "weak" mobility JPs, respectively. All $N = N_w + N_s$ particles are represented by interacting disks of radius r_0 . For very short distances, they interact with each other *via* a truncated Lennard-Jones potential,

$$V_{ij} = 4\epsilon \left[\left(\frac{\sigma}{r_{ij}} \right)^{12} - \left(\frac{\sigma}{r_{ij}} \right)^6 \right], \quad \text{if } r_{ij} \leq r_m \quad (1)$$

$$= 0 \quad \text{otherwise,}$$

where ϵ is the interaction constant, r_m locates the potential minimum, and $\sigma = 2r_0$. Thus, particles interact only through steric repulsion, *i.e.*, no hydrodynamic interactions will be considered here. To illustrate how the motility of the two species is interrelated, we computed two quantifiers, the particle velocity distributions and their effusion rates. However, the former cannot be computed for massless particles (that is in the absence of inertia). Therefore, we assumed damped particle dynamics, although in most practical situations inertia plays no significant role, due to the comparatively very fast viscous relaxation of the suspension medium.⁴⁰ One can recover the standard massless, or overdamped, limit by taking very large values of the damping constant γ . This holds on all physical circumstances when the viscous relaxation time, $1/\gamma$,

is much shorter than any other relevant time scale of the system dynamics.^{42–44}

The dynamics of the particles in the xy -plane can be described by the following set of Langevin equations,

$$m\ddot{x}_i = -\gamma \left[\dot{x}_i + \sum_j F_{ij}^x + v_0 \cos \theta_i + \sqrt{D_0} \xi_i^x(t) \right], \quad (2)$$

$$m\ddot{y}_i = -\gamma \left[\dot{y}_i + \sum_j F_{ij}^y + v_0 \sin \theta_i + \sqrt{D_0} \xi_i^y(t) \right], \quad (3)$$

$$\dot{\theta}_i = \xi_i^\theta. \quad (4)$$

The i -th particle with instantaneous position (x_i, y_i) diffuses under the combined action of self-propulsion and equilibrium thermal fluctuations. Here, (ξ_i^x, ξ_i^y) are the components of the thermal fluctuations responsible for the particle translational diffusion; they are modeled by Gaussian white noises with $\langle \xi_i^\alpha(t) \rangle = 0$ and $\langle \xi_i^\alpha(t) \xi_i^\beta(0) \rangle = 2D_0 \delta_{\alpha\beta} \delta(t)$, where $\alpha, \beta = x, y$. The constant $D_0 = kT/\gamma$ can be computed by measuring the translational diffusion of a free JP in the absence of self-propulsion. Here γ plays the role of an effective damping constant incorporating all environmental interactions not explicitly accounted for in eqn (2) and (3), like fluid viscosity, hydrodynamic drag, surface effects, *etc.* The second term in the right hand side of the same equations represents the repulsive forces derived from the Lennard-Jones pair potential of eqn (1).

The propulsion velocities with modulus v_w and v_s are oriented at an angle θ_i with respect to the laboratory x -axis. Due to the particle rotational diffusion, the angles θ_i change randomly according to the Wiener process of eqn (4), where $\langle \xi_i^\theta(t) \rangle = 0$ and $\langle \xi_i^\theta(t) \xi_i^\theta(0) \rangle = 2D_\theta \delta(t)$. For a passive particle, the rotational diffusion constant, D_θ , is typically related to the viscosity, η_v , and temperature, T , of the suspension medium and to the geometry of the particle itself.²⁹ For spherical colloidal particles with radius r_0 , the rotational diffusion constant can be expressed as $D_\theta = kT/8\pi\eta_v r_0^3$. However, for an active JP rotational diffusion can also depend on the mechanisms fueling its self-propulsion. For this reason, D_0 , v_0 , and D_θ are treated here as independent model parameters.^{4,5,30} Moreover, we assumed for simplicity that the noise parameters D_0 and D_θ are the same for both JP species.

From the correlation function, $\langle \cos \theta_i(t) \cos \theta_i(0) \rangle = \langle \sin \theta_i(t) \sin \theta_i(0) \rangle = (1/2) \exp[-D_\theta |t|]$, it is apparent that D_θ coincides with the rotational relaxation rate of the self-propulsion velocity $\vec{v}_0(t)$. Moreover, we remind that, in the limit of large γ , a non-interacting JP of eqn (2)–(4) diffuses normally with the translational constant, D , consisting of two distinct terms,¹² a thermal and a self-propulsion one, namely $D = D_0 + v_0^2/2D_\theta$.

We numerically integrated eqn (2)–(4) using a standard Milstein algorithm to obtain the velocity distributions and effusion rates of the both mixture species. The numerical integration was performed using a very short time step, 10^{-6} – 10^{-7} , to ensure numerical stability. Computing the velocity distributions requires no confinement scheme. However, to keep

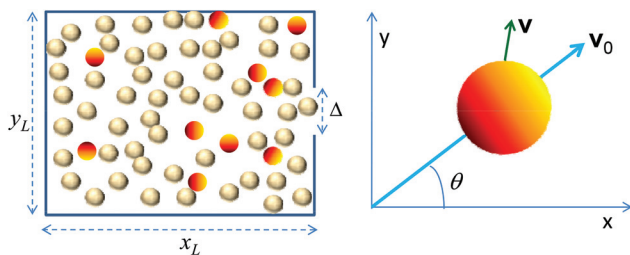


Fig. 1 Left: Schematic of a mixture of self-propelled particles in a rectangular box ($x_L \times y_L$) with an opening of width Δ . Right: Schematic of a two-dimensional self-propelled JP. Its dynamical, \vec{v} , and self-propulsion velocities, \vec{v}_0 , are depicted by distinct vectors.

the mixture densities constant, we set up a simulation box of dimension $x_L \times y_L$ with periodic boundary conditions. Instead, to simulate the effusion rates we assumed that the particle centers are confined inside the simulation box. The particles can then exit the box only through a very small opening of width $\Delta + 2r_0$, to model a pore of accessible width Δ (see Fig. 1). The opening can be centered anywhere along the box wall. Simulating a confined JP requires defining its collisional dynamics at the boundaries. For the translational velocity \vec{v} , we imposed elastic reflection, whereas the rotational coordinate, θ , was assumed not to change upon collision (sliding boundary conditions⁹). As a consequence, an active JP tends to slide along the walls until rotational fluctuations, ξ_θ , redirect the particle inside the box. We computed the effusion rate, defined as the number of particles exiting the box through the pore per unit of time, for different particle swimming properties and confinement geometries. At $t = 0$, the particles were uniformly distributed in the box with random orientation. To keep the number density of both species constant, a particle of the same species was re-injected with a random position and orientation inside the box, whenever one had escaped through the pore. The running time was set to $10^4 \times \tau_\theta$ or 10^4 , whichever was greater, so as to neglect transient effects due to the initial conditions. The data points reported in the figures shown here have been obtained by ensemble averaging over a minimum of 1000 trajectories. For the simulation parameter values adopted here, the time and length scales are seconds and micrometers, respectively. The mass of a silica bead of radius $0.75 \mu\text{m}$ is taken as a unit of mass. Taking the density⁴⁵ of $\text{SiO}_2 \approx 2 \text{ g cm}^{-3}$, the unit of mass would be about $4 \times 10^{-12} \text{ g}$. In rescaled units, parameters used in our simulations are consistent with the corresponding values reported in the experimental literature.

3. Velocity distribution

It is well known that the velocity of overdamped Brownian particles is an ill-defined quantity. Indeed, massless particles undergo a displacement only during the action of external forces,⁴⁰ here thermal fluctuations, collisions against other particles or the box walls, and the effective self-propulsion

forces.⁴¹ Therefore, to extract a velocity distribution, one needs to simulate inertial effects.

By numerically integrating the coupled eqn (2)–(4), we systematically analyzed velocity distributions in systems of non-interacting and interacting active JPs, as well as in binary mixtures of two species of JPs with different self-propulsion speeds.

3.1. Velocity distribution of non-interacting active particles

Let us begin with the case of a single species of non-interacting particles self-propelling in a thermal bath of temperature T with speed v_0 . Velocity distribution at different values of the rotational diffusion constant, D_θ , is shown in Fig. 2. It is apparent that inertial effects become important as the viscous relaxation time constant, $\tau_\gamma = 1/\gamma$, grows comparable to or greater than the rotational relaxation time $\tau_\theta = 1/D_\theta$. When $\tau_\gamma \gg \tau_\theta$ (or $\gamma \ll D_\theta$), the velocity distributions are mostly determined by thermal fluctuations. In the opposite regime, $\tau_\gamma \ll \tau_\theta$ (or $\gamma \gg D_\theta$), self-propulsion effects seem to prevail. Hence, the transition from self-propulsion to the inertia-dominated regime clearly emerges from the velocity distributions of Fig. 2.

Recall that, as anticipated above, for asymptotically large observation times, a free JP behaves like a persistent Brownian particle with effective temperature^{47,48}

$$T_{\text{eff}} = \frac{\gamma}{k} \left(D_0 + \frac{v_0^2}{2D_\theta} \right), \quad (5)$$

and persistence length $l_\theta = v_0 \tau_\theta$. For suitably large values of D_θ , the self-propulsion length is shorter than the free thermal length, \sqrt{mkT}/γ , that is $T_{\text{eff}} \approx T$. As a consequence, one expects that the particle velocities must be distributed according to the two-dimensional Maxwellian function,

$$p(v) = \left(\frac{mv}{kT} \right) \exp \left(-\frac{mv^2}{2kT} \right). \quad (6)$$

This assertion is corroborated by the numerical results of Fig. 2(a and b).

A different type of velocity distribution emerges when the self-propulsion length of the active particle is set much larger than its thermal length. The ensuing velocity distribution is governed by the self-propulsion dynamics, its maximum being centered at around v_0 . Such a distribution results from the combination of the Maxwellian distribution of eqn (6), and a Gaussian distribution with mean v_0 and variance $kT = \gamma D_0$, both due to thermal fluctuations. When lowering the temperature, T , the contribution of the Maxwellian part is quickly suppressed, which results in the 2D Gaussian distribution

$$p(v) = \left(\frac{1}{\sqrt{2\pi\gamma D_0}} \right) \exp \left[-\frac{(v - v_0)^2}{2\gamma D_0} \right]. \quad (7)$$

In the zero temperature limit, that is, when translational noise is negligible with respect to rotational noise, this distribution tends to a δ -function centered at v_0 , whereas the corresponding velocity distributions in one direction become, $p(v_{x,y}) = 1/\pi \sqrt{1 - (v_{x,y}/v_0)^2}$. These properties are confirmed

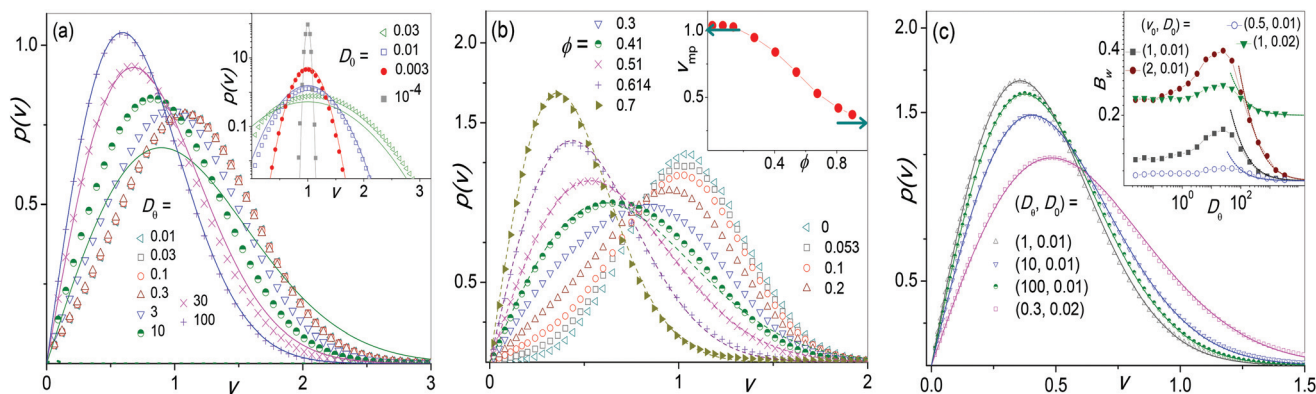


Fig. 2 (a) Velocity distribution of non-interacting active JPs for different D_θ (see legends). The inset illustrates the effect of thermal noise for $D_\theta = 0.3$. Symbols denote numerical simulation data; solid lines are the analytical estimates of eqn (6), main panel, and eqn (7), inset. The parameters used are (unless reported otherwise in the legends): $D_0 = 0.03$, $v_0 = 1$, $\gamma = 10$, $m = 1$. (b) Velocity distribution of interacting self-propelled particles for different packing fractions, ϕ . (c) Velocity distribution of interacting self-propelled particles for different D_θ . In the main panels (b) and (c), solid lines represent the least-squares fitted 2D Gaussian distributions of eqn (8). The parameters used are (unless reported otherwise in the legends): $v_0 = 1$, $\tau_\theta = 3.33$, $\tau_\gamma = 0.1$, $r_0 = 0.75$, $D_0 = 0.01$, $\varepsilon = 1$, $\phi = 0.7$. Insets: (b) most probable velocity, v_{mp} , versus packing fraction. Asymptotes, at $\phi \rightarrow 0$, $v_{mp} \rightarrow v_0$ and for $\phi \rightarrow 1$, $v_{mp} \rightarrow \sqrt{B}$ are depicted by horizontal arrows. (c) Variance of the distribution eqn (8) as a function of D_θ for different values of v_0 and D_0 . Dotted lines are analytical curves corresponding to the effective temperature of eqn (5) (see text).

by the simulation results displayed in Fig. 2(a) and ESI Fig. SM1.†

3.2. Velocity distribution in a system of interacting active particles

Velocity distributions for different values of the packing fraction, $\phi = 4r_0^2 N_l / (x_L + 2r_0)(y_L + 2r_0)$, are displayed in Fig. 2(b). These distributions are centered at v_0 for weakly interacting particles and their center shifts towards lower values with increasing ϕ . As apparent here, in dense systems, say with $\phi > 0.5$, interacting active JPs obey the Maxwellian velocity distribution,

$$p(v) = \frac{v}{B} \exp\left[-\frac{v^2}{2B}\right], \quad (8)$$

where the fitting parameter, B , depends on the bath temperature T , the particle rotational diffusion D_θ and self-propulsion speed v_0 , and the system packing fraction ϕ . For $v_0 \rightarrow 0$, the distribution is insensitive to the pair interaction, so that $B = \gamma D_0$, like in gas kinetic theory. Therefore, the interaction dependence of the velocity distribution is a non-equilibrium effect of self-propulsion. To examine the impact of self-propulsion on the velocity distribution in a dense system, in Fig. 2(c) we plotted $p(v)$ (main panel) and distribution width B (inset) as a function of D_θ for different values of the speed v_0 . One notices immediately that:

(i) For very slow rotational relaxation, the width of the distribution is almost independent of D_θ . In this regime, the self-propulsion length l_θ is much larger than the average effective inter-particle distance l_s , so that the particle free path cannot exceed l_s . The fitting parameter seems to obey the empirical law, $B = \gamma(D_0 + \alpha v^2)$, with α a function of the packing fraction. This result can be explained by comparing B with kT_{eff} in eqn

(5), which we rewrite here as $kT_{\text{eff}} = \gamma(D_0 + v_0^2 \tau_\theta / 2)$. Upon increasing ϕ , both the mean-free ballistic time $\tau_s = l_s / v_0$ and the mean-free diffusion time $\tau_D = l_s^2 / 2D_0$ grow larger than the persistence time τ_θ . As a consequence, τ_θ in the above expression for kT_{eff} should now be replaced by $\bar{\tau} = \min\{\tau_s, \tau_D\}$. When the active suspension is so dense that $D_0 > v_0 l_s / 2$, then $\bar{\tau} = \tau_D$, so that the fitting parameter B depends quadratically on v_0 with α a function of ϕ .

On a closer look, one notices that α also weakly depends on v_0 . This is because self-propulsion makes the colliding particles to occasionally overlap, thus slightly lowering the effective ϕ value. The pair penetration length and, hence, the effective particle size can be estimated by equating the self-propulsion force to the inter-particle repulsion.

(ii) In the opposite limit, $l_\theta < l_s$, the active particles manage to change their direction before colliding with other particles, so that their inter-collisional dynamics is dominated by the self-propulsion dynamics. They behave as if they were floating in a thermal bath with the effective temperature of eqn (5). The ensuing estimates of the distribution fitting parameter, $B = \gamma(D_0 + v^2 \tau_\theta / 2)$, drawn in the inset of Fig. 2(c) fairly agree with the numerical data.

Fig. 2(b and c) [and ESI Fig. SM2†] also suggest that, under the condition that $v_0^2 \gg B$, the most probable value of v , v_{mp} , approaches v_0 . Based on our argument of (i) for dense active suspensions, this requires $v_0^2 \gg \gamma D_0 / (1 - \alpha)$, with $\alpha = l_s^2 \gamma / 4 D_0$. Of course, this estimate holds only for not too large γ values, so that $\alpha < 1$, i.e., for $l_s^2 \gamma / 4 < D_0$.

(iii) In the intermediate regime, the curves B versus D_θ exhibit a maximum. Starting with $l_s \ll l_\theta$, as one increases the rotational diffusion constant, self-propulsion enters gradually into play by *enhancing* B . On the other hand, self-propulsion effects disappear in the diffusive regime, $l_\theta \ll l_s$, where B decreases with increasing D_θ . Not surprisingly, B appears to

reach its maximum in the intermediate regime for l_θ of the order of the mean inter-particle distance l_s .

Finally, it should be noted that the fitting values of B have been extracted by least-squares fitting. The fidelity of such fittings has been assessed by computing the mean square weighted deviation⁴⁶ χ_v^2 . It always returned values close to 1, except for large v_0 . This deviation is noticeable for $v_0 = 4$, where the rotational diffusion is rather low (shown in ESI Fig. SM2†).

3.3. Velocity distribution in a binary mixture of active particles

Let us consider now a mixture of active particles of two types. Let us denote the N_w particles with fixed self-propulsion speed v_w , as *weakly* active, and the remaining N_s particles with tunable self-propulsion velocity v_s , as *strongly* active. A comparison of velocity distributions of the weak (hollow symbols) and strong (solid symbols) JPs in a binary mixture is shown in Fig. 3(a) for different fractions $\eta_s = N_s/N$ of the strong active particles. Plots here correspond to situations where the system packing fraction ϕ is quite large and the velocity distributions $p(v)$ are of the Maxwellian type, eqn (8). As to be expected, the plots in Fig. 3(a) show that weak active particle distributions grow wider, and their maxima shift to higher velocities, with increasing η_s . On the other hand, the distributions of the stronger component shrink and their maxima shift toward lower velocity values in comparison with the single component system. This result suggests an effective *motility transfer* from more active to less active particles. To better characterize the underlying mechanism, we estimated the distribution half-widths B for different mixture compositions. The ratio $B_w(\eta_s)/B_w(0)$ in the inset of Fig. 3(a) grows linearly with η_s , its slope depending on the thermal energy, $kT = \gamma D_0$, and self-propulsion speed of both JP species. This behavior can be explained as follows. Since the system is dense and $l_s \ll l_\theta$, self-propulsion only contributes to

the effective thermal motion of the system, see item (i) of section 3.2. Adding up the average kinetic energy contribution from both species and equating the result to the corresponding prediction based on eqn (8), one can arrive at

$$\frac{B_i(\eta_j)}{B_i(0)} = 1 + \left(\frac{\alpha_j v_j^2 - \alpha_i v_i^2}{\gamma D_0 + \alpha_i v_i^2} \right) \eta_j. \quad (9)$$

where $\{i,j\} = \{s,w\}$ with $i \neq j$. The above estimate rests on the assumption that the self-propulsion contributions to the kinetic energy in this regime are directly proportional to v_i^2 with a proportionality constant α_i . For $l_s \ll l_\theta$, both α_i are insensitive to the rotational diffusion constant D_θ , and weakly depend on v_i . In contrast, for $l_s \gg l_\theta$, $\alpha_w = \alpha_s = \gamma/2D_\theta$.

To better interpret the mechanism of host-guest mobility transfer, in Fig. 3(b) we compare the widths B_s and B_w of the relevant velocity distributions. We simplify our analysis by focusing on the parameter regimes where both mixture components exhibit a Maxwellian velocity distribution. Fig. 3(b) shows that B_w linearly grows as the fraction, η_s , of strong active particles increases. By contrast, B_s decreases with increasing η_w . Eqn (9) is useful to explain the linear dependence of both B_s and B_w on η_s . It is apparent from both numerical simulations and eqn (9) that in a binary mixture the velocity distribution of the weak host depends not as much on its own self-propulsion parameters but on the presence of the strong guest. Under the Maxwellian conditions assumed here, $v_w^2 \ll v_s^2$ and $\gamma D_0 \gg \tau_\theta v_w^2$, one can easily relate the effective temperature of the binary mixture to the distribution widths $B_{s,w}$ as follows,

$$kT_{\text{eff}} = (1 - \eta_s)B_w(\eta_s) + \eta_s B_s(\eta_s). \quad (10)$$

This estimate for T_{eff} is in good agreement with the numerical results shown in Fig. 3(c). In view of the linear η dependence of B , one would then expect T_{eff} to be a nonlinear func-

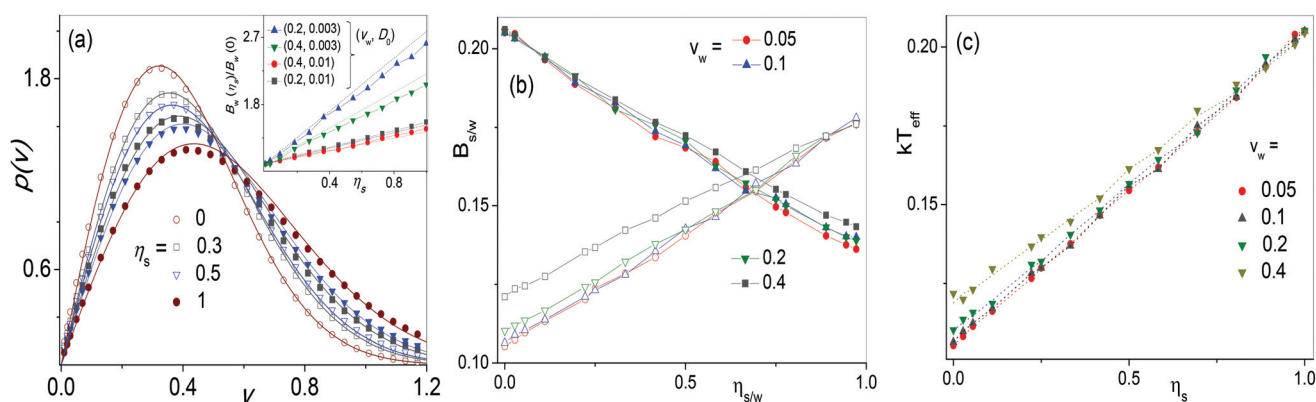


Fig. 3 (a) Comparison of velocity distribution $p(v)$ of weak (empty symbols) and strong (filled symbols) active particles with varying composition η_s of the binary mixture. Note that solid (hollow) circles represent velocity distribution of strong (weak) active particles for the interacting single species case. Solid lines correspond to eqn (8) where B is obtained from least-squares fittings. Inset plots depict the variation of distribution width of weak JPs B_w as a function of the fraction of strong active particles, $\eta_s = N_s/N_t$. Thus, $\eta_s = 0$ means that all particles are weak and $\eta_s = 1$ that all particles are strong. Dotted lines represent eqn (9) with the relevant best-fit parameters α_s and α_w . (b) Distribution widths of weak, B_w (empty symbols), and strong active JPs, B_s (filled symbols), respectively versus η_s and η_w for different v_w . (c) kT_{eff} versus η_s for different v_w : numerical data (symbols) are compared with the analytical estimates of eqn (10) (dotted lines). The remaining model parameters are (unless reported otherwise in the legends): $v_s = 1$, $D_\theta = 0.3$, $\tau_\gamma = 0.1$, $r_0 = 0.75$, $D_0 = 0.01$, $\varepsilon = 1$, and $\phi = 0.61$.

tion of η . However, by inspecting eqn (9) and (10) one easily concludes that, for the simulation parameters adopted in Fig. 3(c), nonlinear corrections are negligible. As a result, the effective temperature of the binary mixture grows (almost) linearly with the molar fraction of the guest particles. Moreover, eqn (9) also hints at how the self-propulsion properties of the host and guest particles impact T_{eff} .

One often needs to know the fraction of *weakly* active particles whose speed exceeds a specified value, say v_c . One can calculate this quantity, $\chi(\eta_s, v_c)$, directly from the velocity distribution function of the less active JPs, that is

$$\chi(\eta_s, v_c) = \int_{v_c}^{\infty} p(v, \eta_s) dv. \quad (11)$$

Thus, $\chi(\eta_s, v_c)$ is the fraction of *weakly* active particles having an instantaneous velocity greater than the cut-off velocity v_c in the binary mixture with N_w weak JPs. To clarify the role of v_c , we consider the kinetic model of reaction rate theory. As the reactant particles collide with each other, only a certain fraction of such collisions leads to the formation of the desired product. For this purpose it is necessary that the energy of the reactants at the moment of the impact exceeds a threshold value, E_a , also known as reaction *activation energy*, which corresponds to the cut-off activation speed, $v_c = \sqrt{2mE_a}$. Therefore, coming back to the problem at hand, it would be desirable to know how the ratio $\chi(\eta_s, v_c)/\chi(0, v_c)$ changes by adding a certain amount of strongly active particles.

For the velocity distributions of eqn (8), such a ratio reads as follows

$$\frac{\chi(\eta_s, v_c)}{\chi(0, v_c)} = \exp\left[-\frac{v_c^2}{2} \left(\frac{1}{B(\eta_s)} - \frac{1}{B(0)}\right)\right]. \quad (12)$$

This quantity, namely the ratio of the number of weakly active JPs with speed larger than v_c to the same number, but in the absence of strongly active JPs, is plotted in Fig. 4 for different values of v_c . Our simulations show that $\chi(\eta_s, v_c)/\chi(0, v_c)$ is a monotonically growing function of η_s ; its growth rate increases with increasing v_c . These observations support the strategy discussed in section 1 aiming at enhancing the motility of weakly

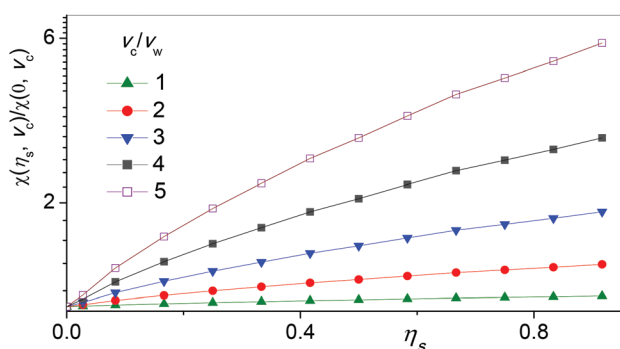


Fig. 4 The ratio, $\chi(\eta_s, v_c)/\chi(0, v_c)$ versus η_s for different v_c . The parameters used are (unless mentioned in the legends): $v_s = 1$, $v_w = 0.2$, $D_\theta = 0.3$, $\tau_r = 0.1$, $r_0 = 0.75$, $D_0 = 0.01$, $\varepsilon = 1$, and $\phi = 0.8$.

active, or even passive particles, by adding to the system a small fraction of strongly active particles as autonomous stirrers.

4. Effusion

In the previous section, we showed how adding a relatively small fraction of highly motile microswimmers to a suspension of less motile microswimmers can considerably enhance the overall motility of the mixture. This effect was demonstrated in the presence of inertia. We consider now the limiting case of overdamped, or massless, active particles. This limit corresponds to low Reynolds numbers, a hydrodynamic regime that applies to most microswimmers investigated in the literature, both biological and artificial. This raises a problem, because, as mentioned above, the velocity distribution of massless particles is mathematically ill-defined. To avoid this difficulty, in our simulations we computed an alternative motility quantifier for the overdamped limit, namely the effusion rate of the active JPs through a narrow pore of the simulation box. The corresponding Langevin equations in the highly damped situation are obtained by ignoring inertia in eqn (2)–(4),

$$\dot{x}_i = \sum_j F_{ij}^x + v_0 \cos \theta_i + \sqrt{D_0} \xi_i^x(t), \quad (13)$$

$$\dot{y}_i = \sum_j F_{ij}^y + v_0 \sin \theta_i + \sqrt{D_0} \xi_i^y(t), \quad (14)$$

$$\dot{\theta}_i = \sqrt{D_\theta} \xi_i^\theta. \quad (15)$$

The effusion rate has been studied in depth to characterize classical transport in constrained geometries.⁵⁰ We define the effusion rate of the *strong* (s) [*weak* (w)] JPs, E_s (E_w), as the number of s (w) particles exiting the simulation box per unit time. In the case of a single-component system, we denote the effusion rate by E_m .

Let us consider the effusion rate $E_m(0)$ of a single species of non-interacting JPs with $\varepsilon = 0$. In Fig. 5(a) we plotted a few curves $E_m(0)$ versus v_0 for different values of D_θ . For $v_0 \rightarrow 0$, the effusion is controlled by thermal motion and, as expected, is insensitive to v_0 . Effects due to self-propulsion become appreciable only for values of v_0 larger than the particle thermal speed $\sqrt{2D_0D_\theta}$. Beyond this critical value, the effusion rate grows first quadratically with v_0 and then saturates toward an asymptotic value. The rising branches occur for $l_\theta \ll x_L, y_L$. Indeed, for very short rotational relaxation times τ_θ , when it can safely be assumed that particles diffuse in a thermal bath with effective constant D_{eff} , the effusion rate through a narrow pore of effective width $\Delta \ll x_L, y_L$, reads as follows^{50–52}

$$E_i = \pi \rho_i D_{\text{eff}} \left[\ln \left(\frac{x_L + y_L}{\Delta} \right) \right]^{-1}. \quad (16)$$

Here, the suffix i refers to either s or w, ρ_i denotes the number density of the mixture component i , and D_{eff} is now $D_0 + v_0^2/2D_\theta$ – see eqn (5). This estimate for $E_i(0)$ agrees fairly closely with the simulation results reported in Fig. 5(a). In the

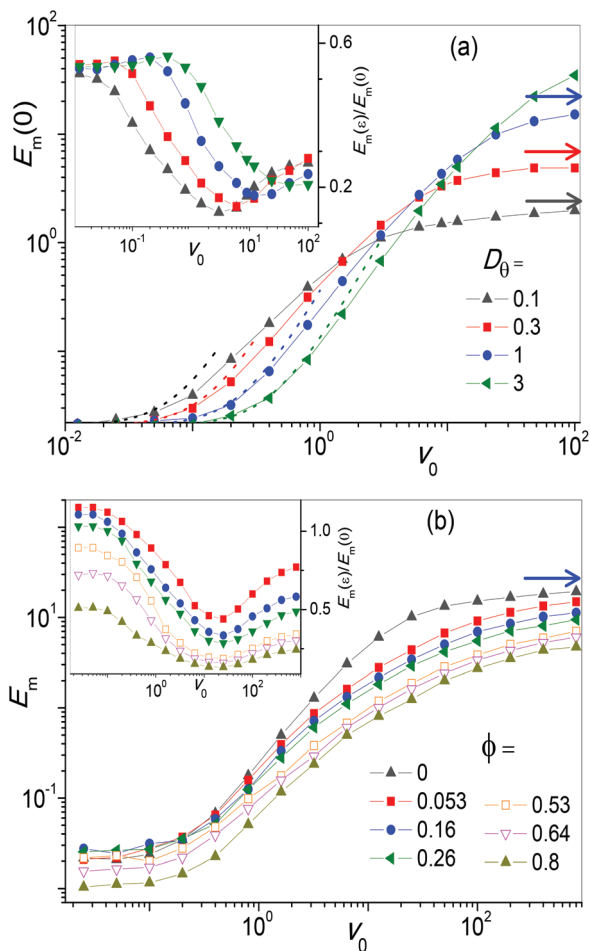


Fig. 5 (a) Effusion rate $E_m(0)$ of non-interacting JPs with $\varepsilon = 0$, as a function of the self-propulsion velocity v_0 for different rotational diffusion coefficient D_θ . Dotted lines are the predictions based on eqn (16). Horizontal arrows indicate the corresponding rate upper bound, eqn (17), for large $\tau_\theta = 1/D_\theta$. Inset: The effusion rate ratio $E_m(\varepsilon)/E_m(0)$ for $\varepsilon = 0.1$ and different D_θ (see legends). (b) Effusion rate $E_m(\varepsilon)$ of interacting self-propelled particles versus v_0 for $\varepsilon = 1$ and different packing fraction ϕ . Inset: $E_m(\varepsilon)/E_m(0)$ versus v_0 for the same set of parameters as the main panel. Other simulation parameters for main panels and inset: $x_L = y_L = 10$, $\Delta = 0.5$, $r_0 = 0.5$, $D_0 = 0.03$, and $N_m = 80$.

opposite rotational regime, when $l_\theta \gg x_L, y_L$, the slow direction changes of the self-propulsion velocity tend to suppress the particle effusion through the pore. Assuming that τ_θ is much larger than any other system time scale, the effusion rate can be approximated by⁵¹

$$E_i(0) \approx x_L y_L \rho_i D_\theta / \pi. \quad (17)$$

This asymptotic estimate has been marked in Fig. 5(a) by horizontal arrows.

The effusion rate of interacting self-propelling particles with $\varepsilon > 0$ is plotted in the inset of Fig. 5(a). This figure shows the v_0 -dependence of the effusion rate relative to the corresponding rate in the absence of interaction, $E_m(\varepsilon)/E_m(0)$, for several values of D_θ . The system we simulated here was quite dense ($\phi = 0.66$), so that the self-propulsion mechanism

becomes strongly constrained, being $l_s \ll l_\theta$. Like in non-interacting systems, the effusion rate is insensitive to self-propulsion with low v_0 . More remarkably, with increasing v_0 the relative effusion decreases.

We attributed this result to the jamming of the interacting particles caused by self-propulsion in the vicinity of the box walls. Snapshots of the mixture configurations [see the inset of Fig 6(b) and ESI Fig. SM3†] corroborate this assertion. The jamming effect becomes noticeable as soon as the self-propulsion length becomes larger than the confining box. Therefore, the appearance of such an effect and minima of $E_m(\varepsilon)/E_m(0)$ versus v_0 are inversely related to the rotational diffusion [see the inset of Fig. 5(a)]. By the same token, one expects that both the decaying and raising branches of the curves $E_m(\varepsilon)/E_m(0)$ versus v_0 are quite insensitive to the packing fraction, ϕ , in

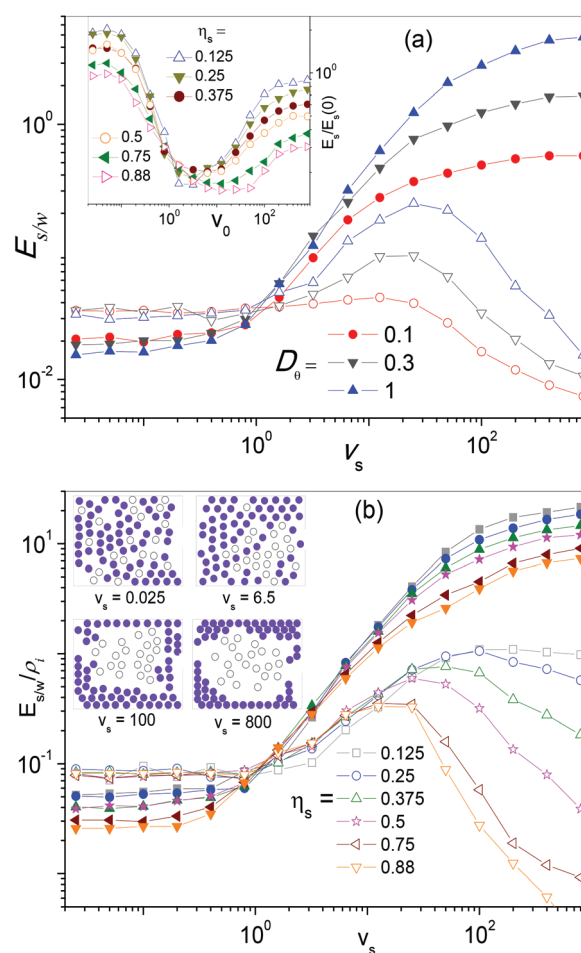


Fig. 6 (a) Effusion rates E_s (filled dots) and E_w (empty dots) versus v_s for binary mixture with $\eta_s = 0.5$ and different values of D_θ (see legends). Inset: Effusion rate ratio of stronger component, $E_m(\varepsilon)/E_m(0)$ versus v_0 for different η_s and $D_\theta = 1$. (b) Effusion rates E_s (filled dots) and E_w (empty dots) versus v_s in a binary mixture for $D_\theta = 1$ and different η_s (see legends). Inset: Snapshot of binary mixture with $\eta_s = 0.75$, $D_\theta = 1$ and different v_s [0.025 (top-left), 6.5 (top-right), 100 (bottom-left), and 800 (bottom-right)]. Filled and empty circles represent strong and weak JPs, respectively. Other simulation parameters for main panels and insets: $v_w = 1$, $\varepsilon = 1$, $x_L = y_L = 10$, $\Delta = 0.5$, $r_0 = 0.5$, $D_0 = 0.03$, and $N_m = 80$.

agreement with the data plotted in the inset of Fig. 5(b). In the very strong self-propulsion regime, both $E_m(\epsilon)$ and $E_m(0)$ tend to saturate [see Fig. 5(b)]. However, $E_m(\epsilon)$ saturates at larger ν_0 values than in the non-interacting case. A plausible explanation is suggested by a comparison of the mixture snapshots. The particles far away from the walls are more mobile and contribute more to the effusion rate; they are not jammed against the walls and “see” a larger opening-width to compartment-size ratio, Δ/y_L . In contrast, particles jammed against the walls tend to clog the box opening. However, the fraction of the more mobile particles drops fast with increasing ν_0 , thus leading to plateaus in the effusion rate in the limit $\nu_0 \rightarrow \infty$.

Fig. 5(b) shows that the clogging mechanism works even at a low packing fraction, though its impact on effusion is reduced. More remarkably, the excluded volume effect becomes apparent for $\nu_0 \rightarrow 0$: the interacting particles become more effusive than the non-interacting ones. In a dilute solution, this effect persists until the self-propulsion length grows larger than the average inter-particle spacing. This explains why, in the presence of strong self-propulsion, the computed effusion ratios still grow with ν_0 , though quite slowly.

Fig. 6(a) illustrates the dependence of the effusion rates of the two active mixture components on their self-propulsion parameters, ν_0 and D_θ . The mixture is of 1:1 molar ratio of strongly (s) and weakly (w) active particles. We kept the self-propulsion speed ν_w fixed and varied ν_s from values lower to values higher than ν_w . First of all, we notice that the effusion rates of both JP species are almost insensitive to the rotational diffusion for $\nu_s \rightarrow 0$, while developing a strong dependence on D_θ in the opposite limit, $\nu_s \rightarrow \infty$. For $\nu_s > 10\nu_w$, at $D_\theta = 1$ the effusion rate is about one order of magnitude larger than that at $D_\theta = 0.1$.

In Fig. 6(b), we examine the consequences of gradually increasing the fraction of guest particles for different values of their self-propulsion speed, ν_s . While all effusion plots exhibit the same general behavior as in Fig 6(a), a few additional features are remarkable:

(i) The effusion rate of the strongly active JPs keeps increasing, but more slowly than $E_m(0)$ in Fig. 5(a), due to their interaction with the less active JPs. In such a limit, the most active particles tend to push the less active ones against the box walls. Moreover, like in one component systems, clogging effects have great impact on the effusion of both the weak and strong active components.

(ii) In contrast, the effusion rate of the weak JPs remains unchanged for ν_s up to ν_w ; upon further increasing ν_s , it goes through a maximum in agreement with the mechanism of effective motility transfer. Again, for very large self-propulsion, $\nu_s \gg x_L D_\theta, x_L D_\theta$, strongly active JPs jam against the container walls, thus pushing the weaker JPs inside [see snapshots of Fig. 6(b) and ESI Fig. SM4†]. Accordingly, the weaker JPs have a small chance to escape through the opening so that effusion becomes drastically suppressed. Moreover, no decaying branch of E_w vs. ν_s is detectable at low η_s . This happens because very few strong JPs cannot possibly confine all weak particles in the box interior.

In conclusion, we stress that adding a small amount of strongly active JPs does suffice to enhance the effusion of sluggish active JPs, but an excess of them can produce the opposite effect! Recall that, as illustrated by our simulation snapshots, the two components of an active binary mixture can separate into two distinct phases, when the self-propulsion length of one component is much larger than the size of the container and the other one much shorter, that is, for $\nu_s/D_\theta \gg x_L, y_L \gg \nu_w/D_\theta$. However, phase segregation should be avoided for better motility transfer.

As shown in Fig. 5(b), there is a window of tunable ν_s , where the effusion rate of the w particles is enhanced by 2 to 7 times, depending on their rotational relaxation time and the composition of the binary mixture. Also, the span of this window is sensitive to the persistence length of self-propelled motion. This striking result confirms that, even in the absence of inertia, the *motility of the more active microswimmers can be effectively transferred to the less active microswimmers*.

In our numerical analysis we assumed the pore to be centered in one side of a square-shaped simulation box. However, sliding boundary conditions as the JPs move against the cavity walls can affect their average effusion rate. Our simulation shows that this may become an issue only at zero temperature. As a matter of fact, thermal fluctuations assist the escape mechanism by enhancing particle diffusion along the boundaries, thus suppressing possible effects related to the cavity geometry and the actual pore location. To verify this point, we simulated the effusion rate (not shown) for a modified box geometry, whereby the escape pore was moved toward one corner; for the simulation parameters of Fig. 5 we detected no appreciable variations of the relevant effusion rates.

5. Conclusions

We have analyzed the effects of active nano/micromotors with tunable high motility in a suspension of particles whose motility cannot be directly controlled. We showed that by injecting a small fraction of more active Janus particles one can substantially enhance the motility of other less active species. Such a motility enhancement was demonstrated for two typical cases: particles with weak inertia, by studying the velocity distributions of both species, and for overdamped particles, by comparing their effusion rates.

Our numerical study proves that in dense binary mixtures of active particles, the width of the velocity distribution of the less active particles linearly grows with the fraction of more active particles. Thus, the number of particles moving with larger velocity is considerably enhanced. Moreover, for an appropriate choice of the mixture parameters, in the overdamped regime the motility transfer from the more active to the less active subsystem can raise the effusion rate of the latter by 2 to 7 times.

Such a technique of motility control can be implemented in a large variety of biological and medical situations, where one wishes to enhance the motility of insufficiently active nano- or

micro-particles. For example, in the case of weakly motile sperm cells, our proposal has advantages over other similar proposals (e.g., using self-propelled metallic rotors trapping sperm cells⁵³), whereby it is substantially less damaging to living swimmers and much easier to implement, as it does not require the fast guest swimmers to localize and trap individual host particles one by one. Another suggestive application of this method of motility transfer is to speed up a chemical reaction involving slowly diffusing nano-particles, by adding a small amount of more active neutral particles as stirrers.⁵⁴

Conflicts of interest

There are no conflicts to declare.

Acknowledgements

We thank RIKEN Hokusai for providing computational resources. P. K. G. is supported by SERB Start-up Research Grant (Young Scientist) No. YSS/2014/000853 and UGC-BSR Start-Up Grant No. F.30-92/2015. D. D. thanks CSIR, New Delhi, India, for support through a Junior Research Fellowship. V. R. M. and F. N. acknowledge support from the Research Foundation-Flanders (FWO-VI) and Japan Society for the Promotion of Science (JSPS) (JSPS-FWO Grant No. VS.059.18N). F. N. is supported in part by the: MURI Center for Dynamic Magneto-Optics via the Air Force Office of Scientific Research (AFOSR) (FA9550-14-1-0040), Army Research Office (ARO) (Grant No. W911NF-18-1-0358), Japan Science and Technology Agency (JST) (via the Q-LEAP program, and the CREST Grant No. JPMJCR1676), Japan Society for the Promotion of Science (JSPS) (JSPS-RFBR Grant No. 17-52-50023, and JSPS-FWO Grant No. VS.059.18N), the RIKEN-AIST Challenge Research Fund, the Foundational Questions Institute (FQXi), and the NTT PHI Laboratory.

References

- 1 *Janus Particle Synthesis, Self-Assembly and Applications*, ed. S. Jiang and S. Granick, RSC, Cambridge, 2012.
- 2 W. F. Paxton, S. Sundararajan, T. E. Mallouk and A. Sen, Chemical locomotion, *Angew. Chem., Int. Ed.*, 2006, **45**, 5420–5429.
- 3 P. Tierno, Recent advances in anisotropic magnetic colloids: realization, assembly and applications, *Phys. Chem. Chem. Phys.*, 2014, **16**, 23515–23528.
- 4 J. G. Gibbs and Y.-P. Zhao, Autonomously motile catalytic nanomotors by bubble propulsion, *Appl. Phys. Lett.*, 2009, **94**, 163104.
- 5 J. R. Howse, R. A. L. Jones, A. J. Ryan, T. Gough, R. Vafabakhsh and R. Golestanian, Self-Motile Colloidal Particles: From Directed Propulsion to Random Walk, *Phys. Rev. Lett.*, 2007, **99**, 048102.
- 6 C. Bechinger, R. Di Leonardo, H. Löwen, C. Reichhardt, G. Volpe and G. Volpe, Active particles in complex and crowded environments, *Rev. Mod. Phys.*, 2016, **88**, 045006.
- 7 S. Ramaswamy, The Mechanics and Statistics of Active Matter, *Annu. Rev. Condens. Matter Phys.*, 2010, **1**, 323–345.
- 8 G. Volpe, I. Buttinoni, D. Vogt, H.-J. Kummerer and C. Bechinger, Microswimmers in patterned environments, *Soft Matter*, 2011, **7**, 8810–8815.
- 9 P. K. Ghosh, V. R. Misko, F. Marchesoni and F. Nori, Self-Propelled Janus Particles in a Ratchet: Numerical Simulations, *Phys. Rev. Lett.*, 2013, **110**, 268301.
- 10 A. M. Pourrahimi and M. Pumera, Multifunctional and self-propelled spherical Janus nano/micromotors: recent advances, *Nanoscale*, 2018, **10**, 16398–16415.
- 11 B. Ai and J.-C. Wu, Transport of active ellipsoidal particles in ratchet potentials, *J. Chem. Phys.*, 2014, **140**, 094103.
- 12 X. Ao, P. K. Ghosh, Y. Li, G. Schmid, P. Hänggi and F. Marchesoni, Active Brownian motion in a narrow channel, *Eur. Phys. J.: Spec. Top.*, 2014, **223**, 3227–3242.
- 13 P. K. Ghosh, P. Hänggi, F. Marchesoni and F. Nori, Giant negative mobility of Janus particles in a corrugated channel, *Phys. Rev. E: Stat., Nonlinear, Soft Matter Phys.*, 2014, **89**, 062115.
- 14 P. K. Ghosh, Y. Li, F. Marchesoni and F. Nori, Pseudochemotactic drifts of artificial microswimmers, *Phys. Rev. E: Stat., Nonlinear, Soft Matter Phys.*, 2015, **92**, 012114.
- 15 A. Geiseler, P. Hänggi, F. Marchesoni, C. Mulhern and S. Savel'ev, Chemotaxis of artificial microswimmers in active density waves, *Phys. Rev. E*, 2016, **94**, 012613.
- 16 H. D. Vuijk, A. Sharma, D. Mondal, J. Sommer and H. Merlitz, Pseudochemotaxis in inhomogeneous active Brownian systems, *Phys. Rev. E*, 2018, **97**, 042612.
- 17 B. Liebchen and H. Löwen, Optimal navigation strategies for active particles, *EPL*, 2019, **127**, 34003.
- 18 J. Wang, *Nanomachines: Fundamentals and Applications*, Wiley-VCH, Weinheim, 2013.
- 19 *Smart Drug Delivery System*, ed. A. D. Sezer, IntechOpen, 2016.
- 20 H. Yu, A. Kopach, V. R. Misko, A. A. Vasylenko, F. Marchesoni, F. Nori, D. Makarov, L. Baraban and G. Cuniberti, Confined catalytic Janus swimmers: geometry-driven rectification transients and directional locking, *Small*, 2016, **12**, 5882–5890.
- 21 Q. Zou, Z. Li, Z. Lu and Z. Sun, Supracolloidal helices from soft Janus particles by tuning the particle softness, *Nanoscale*, 2016, **8**, 4070–4076.
- 22 S. Krishnamurthy, S. Ghosh, D. Chatterji, R. Ganapathy and A. K. Sood, A micrometre-sized heat engine operating between bacterial reservoirs, *Nat. Phys.*, 2016, **12**, 1134.
- 23 T. Debnath and P. K. Ghosh, Activated barrier crossing dynamics of a Janus particle carrying cargo, *Phys. Chem. Chem. Phys.*, 2018, **20**(38), 25069–25077.
- 24 I. Malytska, C. Mzire, M. Kielar, L. Hirsch, G. Wantz, N. Avarvari, A. Kuhn and L. Bouffier, Bipolar Electrochemistry with Organic Single Crystals for Wireless Synthesis of Metal-Organic Janus Objects and Asymmetric

- Photovoltage Generation, *J. Phys. Chem. C*, 2017, **121**, 12921–12927.
- 25 Y. Fily and M. C. Marchetti, Athermal Phase Separation of Self-Propelled Particles with No Alignment, *Phys. Rev. Lett.*, 2012, **108**, 235702.
- 26 I. Buttinoni, J. Bialke, F. Kümmel, H. Löwen, C. Bechinger and T. Speck, Dynamical Clustering and Phase Separation in Suspensions of Self-Propelled Colloidal Particles, *Phys. Rev. Lett.*, 2013, **110**, 238301.
- 27 F. J. Schwarzendahl and M. G. Mazza, Hydrodynamic interactions dominate the structure of active swimmers pair distribution functions, *J. Chem. Phys.*, 2019, **150**, 184902.
- 28 F. J. Schwarzendahl and M. G. Mazza, Maximum in density heterogeneities of active swimmers, *Soft Matter*, 2018, **14**, 4666.
- 29 H. C. Berg, *Random Walks in Biology*, Princeton University Press, 1984.
- 30 S. van Teeffelen and H. Löwen, Dynamics of a Brownian circle swimmer, *Phys. Rev. E: Stat., Nonlinear, Soft Matter Phys.*, 2008, **78**, 020101(R).
- 31 W. Yang, V. R. Misko, F. Marchesoni and F. Nori, Colloidal transport through trap arrays controlled by active microswimmers, *J. Phys.: Condens. Matter*, 2018, **30**, 264004.
- 32 J. Stürmer, M. Seyrich and H. Stark, Chemotaxis in a binary mixture of active and passive particles, *J. Chem. Phys.*, 2019, **150**, 214901.
- 33 S. Lu, Y. Ou and B. Ai, Ratchet transport of an active-passive mixture chain in confined structures, *Physica A*, 2017, **482**, 501–506.
- 34 F. Hauke, H. Löwen and B. Liebchen, Clustering-induced velocity-reversals of active colloids mixed with passive particles, 2019, arXiv:1909.09578.
- 35 L. Wang and J. Simmchen, Interactions of Active Colloids with Passive Tracers, *Condens. Matter*, 2019, **4**(3), 78, DOI: 10.3390/condmat4030078.
- 36 H. R. Jiang, N. Yoshinaga and M. Sano, Active Motion of a Janus Particle by Self-Thermophoresis in a Defocused Laser Beam, *Phys. Rev. Lett.*, 2010, **105**, 268302.
- 37 X. Lin, T. Si, Z. Wu and Q. He, Self-thermophoretic motion of controlled assembled micro-/nanomotors, *Phys. Chem. Chem. Phys.*, 2017, **19**, 23606–23613.
- 38 X. Wang, L. Baraban, V. R. Misko, F. Nori, T. Huang, G. Cuniberti, J. Fassbender and D. Makarov, Visible Light Actuated Efficient Exclusion Between Plasmonic Ag/AgCl Micromotors and Passive Beads, *Small*, 2018, **14**, 1802537, DOI: 10.1002/sml.201802537.
- 39 X. Wang, L. Baraban, A. Nguyen, J. Ge, V. R. Misko, J. Tempere, F. Nori, P. Formanek, T. Huang, G. Cuniberti, J. Fassbender and D. Makarov, High Motility Visible Light Driven Ag/AgCl Janus Micromotors, *Small*, 2018, **14**, 1803613, DOI: 10.1002/sml.201803613.
- 40 C. W. Gardiner, *Handbook of Stochastic Methods*, Springer, Berlin, 2nd edn, 1985.
- 41 B. ten Hagen, R. Wittkowski, D. Takagi, F. Kümmel, C. Bechinger and H. Löwen, Can the self-propulsion of anisotropic microswimmers be described by using forces and torques?, *J. Phys.: Condens. Matter*, 2015, **27**, 194110.
- 42 P. K. Ghosh, P. Hänggi, F. Marchesoni, F. Nori and G. Schmid, Brownian transport in corrugated channels with inertia, *Phys. Rev. E: Stat., Nonlinear, Soft Matter Phys.*, 2012, **86**(2), 021112.
- 43 C. Scholz, S. Jahanshahi, A. Ldov and H. Löwen, Inertial delay of self-propelled particles, *Nat. Commun.*, 2018, **9**, 5156.
- 44 H. Löwen, Inertial effects of self-propelled particles: From active Brownian to active Langevin motion, *J. Chem. Phys.*, 2020, **152**, 040901.
- 45 *CRC Handbook of Chemistry and Physics*, ed. W. M. Haynes, CRC Press, Boca Raton, FL, 2011.
- 46 P. R. Bevington, *Data Reduction and Error Analysis for the Physical Sciences*, McGraw-Hill, New York, 1969, p. 89. For χ^2 tests, χ_v^2 should be approximately equal to one.
- 47 J. Palacci, C. Cottin-Bizonne, C. Ybert and L. Bocquet, Sedimentation and Effective Temperature of Active Colloidal Suspensions, *Phys. Rev. Lett.*, 2010, **105**, 088304.
- 48 J. R. Howse, R. A. L. Jones, A. J. Ryan, T. Gough, R. Vafabakhsh and R. Golestanian, Self-Motile Colloidal Particles: From Directed Propulsion to Random Walk, *Phys. Rev. Lett.*, 2007, **99**, 048102.
- 49 A. Wysocki, R. G. Winkler and G. Gompper, Cooperative motion of active Brownian spheres in three-dimensional dense suspensions, *EPL*, 2014, **105**, 48004.
- 50 D. Holcman and Z. Schuss, *Stochastic Narrow Escape in Molecular and Cellular Biology*, Springer, New York, 2015.
- 51 P. K. Ghosh, Communication: Escape kinetics of self-propelled Janus particles from a cavity: Numerical simulations, *J. Chem. Phys.*, 2014, **141**, 061102.
- 52 L. Bosi, P. K. Ghosh and F. Marchesoni, Analytical estimates of free Brownian diffusion times in corrugated narrow channels, *J. Chem. Phys.*, 2012, **137**, 174110, DOI: 10.1063/1.4764297.
- 53 M. Medina-Sanchez, L. Schwarz, A. K. Meyer, F. Hebenstreit and O. G. Schmidt, Cellular Cargo Delivery: Toward Assisted Fertilization by Sperm Carrying Micromotors, *Nano Lett.*, 2016, **16**, 555.
- 54 S. Sengupta, K. K. Dey, H. S. Muddana, T. Tabouillot, M. E. Ibele, P. J. Butler and A. Sen, Enzyme Molecules as Nanomotors, *J. Am. Chem. Soc.*, 2013, **135**, 1406–1414.